Design of step-stress accelerated life tests for estimating the fatigue reliability of structural components based on a finite-element approach

Jernej Klemenc*, Marko Nagode

University of Ljubljana, Faculty of Mechanical Engineering, Askerceva 6, SI-1000 Ljubljana, Slovenia

Abstract

This article describes how a step-stress accelerated life test (SSALT) can be designed for testing the fatigue life and reliability of structural components with a single failure mode. With simple numerical simulations of the crack's propagation in the notched area of the structural part for different loading levels, the slope of the S-N curve for a structural component is initially estimated. Then, a very few fatigue-life experiments are carried out in the high-cycle domain to determine the intercept of the structure's S-N curve. By considering the scatter from the material's P-S-N curve, different SSALT designs for the structural component can be composed and checked for their expected acceleration factor. The procedure is experimentally validated for the case of a notched specimen and two different SSALT designs. From the results it can be concluded that the predicted durations of the SSALT experiments correlate well with the real experiments.

Key words: Fatigue life reliability, Finite element simulation, Fatigue testing, Weibull distribution, S–N curve, Step loading

Nomenclature

a_0 … constant coefficient for calculating the Weibull's scale parameter $\eta(S_a)$

a_1 … linear coefficient for calculating the Weibull's scale parameter $\eta(S_a)$

b … high-cycle domain exponent of the Coffin-Manson curve

c … low-cycle domain exponent of the Coffin-Manson curve

f … probability density function

fl … index of the loading level at which fatigue failure occurred for the l-th experiment

i, j … index of the loading level

l … index of the sample point

* Author for correspondence; e-mail: jernej.klemenc@fs.uni-lj.si, phone: ++386-1-4771-504, fax: ++386-1-2518-567

$l$min … SSALT starting loading level for the l-th experiment

$l$max … SSALT ending loading level for the l-th experiment

n … number of data points in a sample set

n' … parameter of the Ramberg-Osgood material model

p … probability of rupture, percentile of a time to failure

res … index of residuum

AF … acceleration factor of the SSALT design

E … Young's modulus

F … cumulative distribution function

K … parameter of the Ramberg-Osgood material model

N … total number of load cycles to failure

N_{eq} … equivalent number of load cycles to failure

N_{tot} … number of load cycles in one block of the SSALT

R … reliability

S … loading level

L … log-likelihood cost function

S … set of experimental data

β, η … shape and scale parameter of the Weibull's probability distribution

ε … strain

ε_f … plastic-strain-related intercept of the Coffin-Manson curve

δ … run-out indicator for a fatigue-life data point

σ … stress

σ_f … elastic-stress-related intercept of the Coffin-Manson curve

1 Introduction

The fatigue life of a structural component depends on its geometry, the applied cyclic loads and the material's endurance (Haibach1, Tomazincic et al.2). To minimise the experimental effort and cost, accelerated life and/or reliability tests (ALTs) are widely applied in various industries. One of the first systematic overviews of ALT methods was made by Yurkowski in 19673. Since then, theory

and practice in the field of ALTs have been the subject of thorough research. In previous years a number of review articles on this topic were published, i.e., Escobar and Meeker4, Ma5 and Chen et al.6, while a handbook with a comprehensive description of the ALT methods was published by Nelson in 20047. The methods were developed to cope with a wide range of engineering ALT-related challenges, from single-failure-mode cases (e.g., Cheon et al.8), competing-failure-mode cases (e.g., Bunea and Mazzuchi9, Luo et al.10), optimal ALT designs for model discrimination (Nassir and Pan11), progressive ALT designs (Sha12), etc. Applications of ALT testing on real-case structures have been reported in the field of agriculture (Mattetti et al.13, Paraforos et al.14), the automotive (Putra et al.15, Shafiullah and Wu16) and railway industries (Lu et al.17). It can be concluded that authors have applied different approaches and statistical tools for the design and implementation of accelerated reliability testing.

The objective of our research was to develop the ALT technique that enables time- and cost effective reliability estimation of simple components that are loaded with dynamic loads. The durability of such structural components in the high-cycle fatigue domain for an arbitrary probability of failure/survival can be modelled with S-N curves and their scatter (i.e., the P-S-N curves - see the ASTM E 739-91 standard18 or Klemenc19). When following the approach of Klemenc19, a fatigue-life curve and its scatter for a structure in the high-cycle fatigue domain is represented by a conditional Weibull's20 probability density function (PDF):

$$f(N \mid S) = \frac{\beta}{\eta(S)} \cdot \left(\frac{N}{\eta(S)} \right)^{\beta-1} \cdot \exp\left[-\left(\frac{N}{\eta(S)} \right)^{\beta} \right] \; ; \; N, \beta, \eta > 0 \qquad (1).$$

where S is the loading level, N is the number of loading cycles to failure at the loading level S, β is the scale parameter of the Weibull's PDF and η is its scale parameter, which is dependent on the loading level S according to the inverse power-law (or Basquin) equation:

$$\eta(S) = 10^{a_0 + a_1 \cdot \log(S)} \; ; \; a_0 > 0, a_1 < 0 \qquad (2)$$

In this model the scale parameter β is constant in the target domain of the loading levels S_a. Therefore, the scattered fatigue-life curve that is used to estimate the component's fatigue reliability is modelled with three parameters: a_0, a_1 and β. The main issue related to the mechanical product design and development is that the P-S-N curve of a product can differ significantly from the P-S-N curve of the applied material due to the component's geometry and manufacturing process. The proposed approach represents a background for a sound design of fatigue-life and reliability testing procedures without any prior knowledge of the component's P-S-N curve.

The step-stress accelerated life/reliability tests (SSALTs) are frequently used in practice for testing structural components with a predominant (or single) failure mode. Since it was shown in the past

that they can offer a significant reduction in the experimental time and cost, if they are properly designed, they are the focus of our research. An overview of the SSALT designs can be found in Li21, Liu22 or El-Din et al.23. SSALT designs are made for different statistical distributions of failure data, many of them are based on Weibull's PDF, but some exceptions also deal with Frechet data (Hakamiopur and Rezaei24) or the Lomax distribution (Elfattah et al.25). Basically, the SSALT designs can be divided into two main groups. The simple SSALT schemes are designed to estimate the reliability of a component at a specified loading level by assuming that the durability curve is (at least broadly) known in advance. Welded structural components are typical candidates for such SSALT schemes, because a weld is usually the weakest part of the structure and the slope of the weld fatigue-life curve is typically equal to 3.0 or 5.0 (see the EUROCODE 3-1.9 standard for details). Lu et al.17 used such a simple SSALT scheme to estimate the reliability of a railway bogie. The theoretical approaches to obtain such SSALT designs generally follow the principle of minimising the asymptotic variance of the maximum likelihood estimates of the model's parameters via calculating Fisher information matrix (Yuan et al.26, Arefi and Razmkhah27, Tang et al.28, Xu and Hunt29, Wang et al.30). If the pre-assigned stress levels for SSALT are applied, only the time limits at certain loading levels S_i are estimated by this minimisation process28. The corresponding optimal SSALT plans are valid for a particular percentile p of a time-to-failure at a pre-specified loading level S_0. They depend on the pre-estimated model parameters. However, these parameter values can be uncertain and the researchers apply either a sensitivity analysis or Bayesian approach to evaluate the uncertainty26. Consequently, this approach is inherently applicable for a reliability demonstration purpose during the late phases of product design or during a serial production. In contrast to the above, it is much more difficult to design the SSALT schemes that are applied to estimate the complete P-S-N curve of the structural component, if no assumptions or pre-estimation experiment are made about the parameters of the durability-curve model. This is the case of initial prototype testing in early phases of the product design. We will show in this article that with a proper combination of experiments, numerical simulations and data analyses, it is possible to compose appropriate SSALT designs of this type, even in the case where the durability-curve trend is not known.

A theoretical foundation for estimating the parameters of the durability-curve and its scatter on the basis of the existing SSALT results was set up by Nelson31. In his research, the inverse power-law equation, the Weibull's PDF and the SSALT scheme were combined to determine the reliability of some electronic components. Later on, the presumptions of Nelson31 that are based on the linear damage-accumulation rule (LDR) were tested against the more complex damage-curve analysis (DCA) and double linear damage rule (DLDR) by Lee and Mu32. The DCA and DLDR approaches performed slightly better than the original approach proposed by Nelson31. However, the

conclusion was that the simplicity of the LDR makes it especially useful for the SSALT, because the reliability estimations were not significantly worse for much less effort that was needed for the test design32. Unfortunately, both publications lack the information on designing the optimal SSALT experiment for the purpose of estimating the complete component's P-S-N curve.

In this article we will show, how SSALT scheme for estimating the structure's P-S-N curve are set-up, if no prior data or information about the structural durability exist. The presented methodology is based on the Nelson's theoretical foundations31. The SSALT scheme is composed with a help of a synthetic P-S-N curve of the structure – see Fig. 1.

Fig. 1: Estimating the component's P-S-N curve via SSALT experiments

To obtain the synthetic P-S-N curve of the structure its slope a_1 is first estimated using the finite element simulations for predicting the crack growth. This is followed by a few fatigue experiments for the notched part at a high loading level to assess an approximate intercept a_0 of the fatigue-life curve from equation (2). These experiments are rather necessary, because most of the existing numerical methods for calculating the fatigue life are too conservative. The scatter of the synthetic P-S-N curve follows the model in equation (1) with the shape parameter β being equal to the shape parameter of the material's P-S-N curve. Since the complete P-S-N curve needs to be estimated, the before-mentioned asymptotic-variance optimisation schemes cannot be applied. Instead, the SSALT scheme is composed manually. However, the synthetic P-S-N curve enables simulating the outcomes of different SSALT schemes and determination of the corresponding acceleration factors.

The article is structured as follows. First, the theoretical background is explained, which is related to: i.) the experimental-numerical estimation of the synthetic fatigue-life curve with the up-front evaluation of different SSALT block designs; ii.) estimating the P-S-N durability curve from SSALT data with Nelson's method; and iii.) estimating the confidence interval for the P-S-N curve. In the third section the experimental and numerical data are presented. This is followed by the results and discussion section. The article finishes with a concluding section, acknowledgments, conflict-of-interest statement and a list of references.

2 Theoretical background

2.1 FE-based design of step-stress accelerated life test

To design an appropriate SSALT for the structural component, its P-S-N curve should be at least approximately known. However, during the design process the real P-S-N curve can be estimated only after the first prototypes are built and tested. Since the prototype components are expensive and their number is usually small, they cannot be wasted just for designing the appropriate SSALT.

The fatigue of structural components is mainly governed by their fatigue-notch factor K_f. The practical rule for its determination is that the static strength of the component (or the fatigue strength at approx. 10^3 load cycles) is linked with a linear function in the log–log diagram with the fatigue strength at 10^6–10^8 load cycles (see Stephenson et al.33). This means that the fatigue-notch factor K_f strongly depends on the loading level in the high-cycle domain. It is close to one during the static loading and can be much larger than one near the fatigue limit. Such an approach represents a significant waste of time and resources, because the experiments need to be done in the low-cycle fatigue domain and near the fatigue-endurance domain. Only after the factor K_f is estimated can the parameters a_0 and a_1 that describe the S-N curve of the structural component be determined. A lot of time and resources are saved if the approximate values of the parameters a_0, a_1 and β from equation (1) are estimated with a combination of the numerical approach and very few fatigue-life experiments near the low-cycle fatigue domain as follows.

Estimating the slope of the component's P-S-N curve

The slope parameter a_0 of the P-S-N curve for the structural component with a single failure mode is estimated using a series of finite-element (FE) simulations as follows:

1. The data for the structure's material that need to be determined up-front are the following: static or cyclic σ-ε diagram and Coffin-Manson curve with scatter34.
2. Using FE simulations the fatigue life of the structural component is predicted at its hot-spot for at least two different loading levels in the high-cycle fatigue domain. It is important that the fatigue life is estimated for the phase of crack initiation and the phase of crack growth. In our case the crack-growth was simulated by deleting the finite elements with an average fatigue damage larger than 0.3 for the given number of the load cycles (see Franko et al. for the details of this criterion35).
3. By knowing the simulated fatigue life at different loading levels, the slope a_1 of the S-N curve can be calculated as presented in section 3.2.

Estimating the intercept of the component's P-S-N curve

Knowing the slope a_1 of the component's P-S-N curve, its intercept a_0 can be estimated by one or two fatigue-life experiment(s) at one high loading level. If N_1 is the (average) measured number of the load cycles to failure at the loading level S_1, the parameter a_0 equals – see also equation (2):

$$a_0 = \log(N_1) - a_1 \cdot \log(S_1) \tag{3}$$

Estimating the scatter of the component's P-S-N curve

To predict in advance the scatter of the component's fatigue-life curve, a simple assumption is made, i.e., the shape parameter β of the component's S-N curve is approximately the same as the shape parameter of the component's basic material. At this point the following remark need to be made: if the component has more than one significant failure mode such presumption has a very limited validity.

Simulating the SSALT experiments and estimating SSALT acceleration factor

The estimated parameters a_0, a_1 and β of the component's synthetic P-S-N curve are then used for the purposes of designing the SSALT schemes. The conventional SSALT design is structured in such a way that the current loading level S_i is increased to the next loading level S_{i+1} if the tested sample survives a predefined number of load cycles $N_{\text{tot},i}$ at the current loading level i (see Fig. 2).

Fig. 2: SSALT test plan and the calculation of the equivalent number of load cycles

The first loading level S_1 may be chosen as a normal working load, while the final (the highest) loading level $S_{i\,\max}$ may represent the load, which still results in the same damage mechanism, but at very short fatigue life. After the loading levels S_i and the corresponding block sizes $N_{\text{tot},i}$ of the SSALT are selected by the expert, the corresponding fatigue-life experiments can be simulated using a Weibull's random generator that is based on equations (1) and (2) as follows:

1. The total number of experiments n is chosen for the SSALT design being considered.
2. The SSALT experiments should start at different starting loading levels $S_{l\min}$; $l = 1,\ldots,n$. This means that only a fraction of the n experiments start at a particular loading level $l$min.
3. For each experiment l, its fatigue life N_l is generated according to its starting loading level $S_{l\min}$ with the Weibull's random-number generator, the shape factor of which is equal to β and the scale factor η equal to:

$$\eta(S) = \eta(S_{l\,\min}) = 10^{a_0 + a_1 \cdot \log(S_{l\,\min})} \qquad (4)$$

4. This randomly generated fatigue life N_l is distributed over the initial and the following loading levels until the load-specific equivalent of N_l is consumed. For example:
    a. Suppose that $N_l > N_{\text{tot},l\min}$. This means that at the starting loading level $N_{\text{tot},l\min}$ load cycles are reached without fatigue failure.
    b. The residual load cycles $N_{l\,\min,\text{res}} = N_l - N_{\text{tot},l\,\min}$ are consumed on the following loading levels. The equivalent number of the residual load cycles $N_{l\min,\text{res}}$ at the next loading level $S_{l\min+1}$ is calculated following the Basquin's relation in equation (6):

$$N_{l\min+1,\mathrm{eq}} = N_{l\min,\mathrm{res}} \cdot \left(\frac{S_{l\min+1}}{S_{l\min}} \right)^{a_1} \tag{5}$$

c. If $N_{l\min+1,\mathrm{eq}} < N_{\mathrm{tot},l\min+1}$ the fatigue failure should occur at the loading level $S_{l\min+1}$. Otherwise, all the load cycles at this loading level are consumed and the test is continued at the next loading level $S_{l\min+2}$ with the residual loading cycles from the current loading level equal to $N_{l\min+1,\mathrm{res}} = N_{l\min+1,\mathrm{eq}} - N_{\mathrm{tot},l\min+1}$.

d. The steps b. and c. are continued until the loading level where either the fatigue failure or the limiting condition occurs.

5. Steps 3. and 4. are repeated for every simulated data point.

Finally, the SSALT acceleration factor is determined, which is the ratio between the cumulative number of randomly generated load cycles without the SSALT arrangement (i.e., $\sum_{l=1}^{n} N_l$) and the corresponding step-stress-dependent loading cycles according to the considered SSALT design.

2.2 Statistical concept of SSALT for structural components

The concept of estimating the parameters of the P-S-N curve from a series of the SSALT experiments for single-failure-mode products was presented by Nelson[7,31], who applied the inverse power law, as presented in equation (2), to link the product's load to its service life. When combining the inverse power-law equation with the Weibull's PDF, as in equation (1), it is possible to estimate the product's reliability. To shorten the testing time the fatigue-life experiments are often terminated after a predefined number of loading cycles at the highest loading level $S_{i\,\max}$. Consequently, the sample set comprises complete and incomplete (i.e., censored) data.

To estimate the P-S-N curve for the structural parts, the equivalent number of load cycles to failure at the highest achieved loading level $S_{l\,\max}$ must first be calculated for each experiment $l = 1,\ldots,n$. The highest loading level $S_{l\,\max}$ is the one at which the fatigue failure occurred or the SSALT limit condition was reached. For the particular SSALT design, the load cycles N_{i-1} from the previous loading level S_{i-1} are translated to the equivalent load cycles $N_{i-1,\mathrm{eq}}$ at the current loading level S_i according to the slope a_1 of the S-N curve from equation (2) – see also Fig. 2 and equation (5):

$$N_{i-1,\mathrm{eq}} = N_{i-1} \cdot \left(\frac{S_i}{S_{i-1}} \right)^{a_1} \tag{6}$$

This procedure is repeated up to the highest loading level. Depending on the loading level of the fatigue failure (or the run-out) the corresponding cumulative density function (CDF) is determined on the basis of equations (1) and (2) – see Nelson31 and Fig. 3:

$$F_i(N) = 1 - \exp\left[-\left(\frac{N}{\eta(S_i)}\right)^{\beta}\right] \tag{7}$$

Fig. 3: Determination of the cumulative density function during the SSALT data processing

If the tested sample fails at the 1st loading level, the corresponding terms in equation (7) are:

$$N = N_1 \le N_{\text{tot},1} \tag{8}$$

$$\eta(S_1) = 10^{a_0 + a_1 \cdot \log(S_1)} \tag{9}$$

If the tested sample fails at the 2nd loading level, the corresponding terms in equation (7) are:

$$N = N_2 + N_{1,\text{eq}} \;;\; N_2 \le N_{\text{tot},2} \tag{10}$$

$$\eta(S_2) = 10^{a_0 + a_1 \cdot \log(S_2)} \tag{11}$$

The quantity $N_{1,\text{eq}}$ in equation (10) is calculated with equation (6). Equations (10) to (11) can be written in a general form for an arbitrary loading level of fatigue failure $i > 1$:

$$N = N_i + \sum_{j=1}^{i-1} N_{j,\text{eq}} \;;\; N_i \le N_{\text{tot},i} \tag{12}$$

$$N_{j,\text{eq}} = N_j \cdot \left(\frac{S_i}{S_j}\right)^{a_1} \tag{13}$$

$$\eta(S_i) = 10^{a_0 + a_1 \cdot \log(S_i)} \tag{14}$$

Therefore, at every loading level $i > 1$ the following relation holds:

$$F_{i-1}\left(N_{\text{tot},i-1} + \sum_{\substack{j=1 \\ i>2}}^{i-2} N_{j,\text{eq}}\right) = F_i\left(\sum_{j=1}^{i-1} N_{j,\text{eq}}\right) \tag{15}$$

For each CDF $F_i(N)$, the corresponding PDF $f_i(N)$ can be written as follows, with the number of load cycles to failure N and the scale factor η defined in equations (12) and (14), respectively:

$$f_i(N) = \frac{\beta}{\eta(S_i)} \cdot \left(\frac{N}{\eta(S_i)}\right)^{\beta-1} \cdot \exp\left[-\left(\frac{N}{\eta(S_i)}\right)^{\beta}\right] \tag{16}$$

The result of the series of SSALT experiments is a sample set **S** with n data points:

$$\mathbf{S} = \left\{\left(l\min, l\max, fl, N_{fl}, \delta_l\right); l = 1,...,n\right\} \tag{17}$$

l min and $l$max are the SSALT starting and ending loading levels for the l-th experiment, fl is the index of the loading level at which fatigue failure (or run-out) occurred, N_{fl} is the number of load cycles to failure at the loading level lf and δ_l is an indicator of the fatigue failure:

$$\delta_l = \begin{cases} 1\ ;\ \text{fatigue failure} \\ 0\ ;\ \text{no fatigue failure (run - out)} \end{cases} \tag{18}$$

To estimate the parameters of the Weibull's PDF on the basis of the set with complete and censored data, a modified Maximum Likelihood Function L is used - see Nelson and Meeker [36] or Pascual and Meeker [37] for details:

$$L(a_0, a_1, \beta) = \sum_{l=1}^{n} \left(\delta_l \cdot \ln\left[f_{\text{fl}}(N) \right] + (1 - \delta_l) \cdot \ln\left[1 - F_{\text{fl}}(N) \right] \right) \tag{19}$$

This approach was successfully applied before by Klemenc19 to estimate the P-S-N curve model in equations (1) and (2) on the basis of the constant stress-amplitude experiments. The same objective is followed here, i.e., the optimum parameters a_0, a_1 and β of the component's P-S-N curve should maximise the cost function L in equation (19) with the SSALT data set **S** representing the input. To begin the optimisation process the equivalent number of cycles to failure N are calculated for each experimental result l in the sample set **S** using equations (12) and (13) and initial values of the parameters a_0, a_1 and β. Then, the two functions $f_{\text{fl}}(N)$ and $F_{\text{fl}}(N)$ are determined with equations (16) and (7) and the scale parameter $\eta(S_{\text{fl}})$ calculated using equation (14). The optimum values of the parameters a_0, a_1 and β are estimated using evolutionary algorithms in the same manner as in Klemenc19[38] or Klemenc and Fajdiga34. Two optimisation algorithms were applied, i.e., a real-valued genetic algorithm and a differential ant-stigmergy algorithm. The details can be found in Klemenc19, and so will not be given here.

2.3 Estimating the confidence interval for the SSALT experimental data

As opposed to testing of the electronic components (e.g. see Nelson and Meeker36), testing the prototypes of the mechanical components is limited in time and number, especially in the early phases of product development. Consequently, the estimated parameters of the applied statistical models are uncertain. This uncertainty is assessed via the confidence intervals that are determined for the selected probability of failure at the specified risk level. For the Weibull's PDF different approaches for calculating the confidence intervals have been reported (see Harter and Moore39, Thoman et al.40, McCool41 or Phan and McCool42, Meeker and Escobar43). To calculate the confidence intervals for the Weibull's PDF with the non-constant scale parameter η also Monte-Carlo simulations can be applied (Nelson and Meeker36). Since this approach was applied in our case it is briefly described in the continuation.

After the component's P-S-N curve is determined by estimating its parameters a_0, a_1 and β, as described in Section 2.1 from the SSALT sample set $\mathbf{S} = \{(l\min, l\max, fl, N_{fl}, \delta_l); l = 1,...,n\}$, a confidence interval can be determined for the arbitrary probability of a failure p. When following the Monte-Carlo approach, a specified number of data sets with n samples are first simulated using the procedure from Section 2.2. However, in this case the real parameters a_0, a_1 and β are used instead of the synthetic values. In our case 1000 different sample sets of size n were generated for the purpose of the confidence-interval estimation. For each randomly generated data set the parameters a_0, a_1 and β are estimated using the procedure from Section 2.1. Then the fatigue lives $N_{\mathrm{p},i}$ for the probability of rupture p at loading levels i are calculated by rearranging equation (7):

$$\begin{aligned} & p = F_i(N_{\mathrm{p},i}) = 1 - \exp\left[-\left(\frac{N_{\mathrm{p},i}}{\eta(S_i)}\right)^{\beta}\right] \Rightarrow \\ & \Rightarrow \log_{10}(N_{\mathrm{p},i}) = a_0 + a_1 \cdot \log_{10}(S_i) + \frac{1}{\beta} \cdot \log_{10}[-\ln(1-p)] \end{aligned} \tag{20}$$

The 1000 calculated $N_{\mathrm{p},i}$ values at every loading level i are finally approximated with a Weibull's probability distribution from which the one- or two-sided confidence interval is determined for a predefined risk probability.

3 Description of the experimental and numerical data

3.1 Experimental cyclic and Coffin Manson curves of the base material

In our research an advanced, high-strength steel of CP800W-equivalent grade was used for all the experiments. To enable simulations for assessing the synthetic parameters a_0, a_1 and β of the notched component, the material's cyclic and Coffin-Manson curves were first determined.

The cyclic curve was estimated based on fully reversal, strain-controlled, low-cycle fatigue experiments. In 19 cases of the low-cycle fatigue experiments the specimens were loaded with a constant strain amplitude and in seven cases the strain amplitude ε_a was increased by a constant value after every 20 load cycles. In each case the low-cycle fatigue experiments were terminated when the fatigue failure occurred. The low-cycle fatigue experiments were performed for different strain amplitudes ε_a in the range of 0.04% to 2%. The specimens were cut with a water-jet machine from 2.6-mm-thick sheet-metal plate at angles of 0°, 45° and 90° relative to the rolling direction. The low-cycle fatigue specimens were dog-bone shaped with dimensions according to the ASTM E606 standard44 (see the middle part of Fig. 4). The specimens were not additionally treated to reduce their roughness.

Fig. 4: Smooth specimen geometries for high-cycle fatigue testing (top), static and low-cycle fatigue testing (middle) and notched specimen geometry for high-cycle fatigue testing (bottom)

All the low-cycle fatigue experiments were carried out on an MTS Landmark 100-kN hydraulic testing machine. The force was measured with a 100-kN MTS load cell and the strains were measured with a mechanical extensometer MTS 834.11F-24 with a gauge length of 20 mm that was attached to the middle part of the specimen. During the low-cycle fatigue experiments a special guiding device was applied to prevent any buckling of the specimens. The details of the design of the guiding device can be found in Seruga et al.45, and so will not be given here.

From the low-cycle fatigue experiments the average Ramberg-Osgood cyclic curve was modelled; it is presented in Fig. 5 together with all the experimental data points. The parameters of the Ramberg-Osgood material model in the form of $\varepsilon = \sigma/E + K \cdot (\sigma/E)^{n'}$, which were estimated with a least-squares method, are the following: $E = 210$ GPa, $K = 1.46 \cdot 10^{26}$ and $n' = 11.59$. This cyclic curve was then transformed into a true-stress–true-strain form for the FE simulations.

Fig. 5: Cyclic curve (left) and Coffin-Manson curve (right) for the CP800W-equivalent steel

For the Coffin-Manson curve the 19 fully reversal, constant-strain-amplitude, low-cycle fatigue experiments were considered. In addition, 31 force-controlled, fully reversal, high-cycle fatigue experiments were carried out on the same MTS Landmark 100-kN hydraulic testing machine. All the high-cycle fatigue experiments were of constant stress amplitude σ_a in the range 320–450 MPa. The high-cycle fatigue specimens were cut with a water-jet machine from the same 2.6-mm-thick sheet-metal plate at angles of 0°, 45° and 90° relative to the rolling direction. They were dog-bone shaped, as presented at the top of Fig. 4, and were not additionally treated to reduce their roughness. For the purposes of estimating the Coffin-Manson curve, the stress amplitude was transformed into the corresponding strain amplitude using Hooke's law: $\varepsilon_a = \sigma_a / E$. From these 50 low- and high-cycle fatigue experiments, the average Coffin-Manson curve was modelled. It is presented in Fig. 5, together with the experimental data points. The Coffin-Manson curve:

$$\varepsilon_a = \frac{\sigma_f}{E} \cdot (2 \cdot N)^b + \varepsilon_f \cdot (2 \cdot N)^c \tag{21}$$

is described by four parameters b, c, σ_f and ε_f if the Young's modulus E of the material is known. ε_a is the strain amplitude that corresponds to the number of load cycles to failure N. The four parameters were estimated with the least-squares method using a real-valued genetic algorithm. Their values are as follows: $b = -0.084$, $c = -0.834$, $\sigma_f = 1143.2$ MPa and $\varepsilon_f = 0.8$.

For the component's synthetic P-S-N curve, the scatter of the material's S-N curve also needs to be determined for the high-cycle fatigue domain. To apply the model from equations (1) and (2) to the

material's high-cycle fatigue data, only the two parameters a_0 and β need to be determined, because it follows from equation (21) that the slope of the material's S-N curve in the log–log diagram is equal to $a_1 = 1/b = -11.905$. The two parameters a_0 and β were then estimated on the basis of the above-mentioned 31 high-cycle fatigue data using the procedure of Klemenc19. The intercept of the scale parameter η for the S-N curve of the CP800W-equivalent steel in the log–log space is a_0 = 36.264, and the shape parameter of the conditional Weibull's PDF is β= 2.440.

3.2 SSALT design using synthetic P-S-N curve from FE simulations

To validate the SSALT design methodology, which was proposed in Section 2, a simple notched specimen was designed (see the bottom part of Fig. 4). The hole with a diameter of 3 mm in the middle of the specimen ensures that the crack initiation and propagation spot is well controlled. The real specimens were cut from the 2.6-mm-thick sheet-metal plate made from the CP800W-equivalent steel. A 3D model of the specimen was built in Catia V5. The Abaqus CAE 2017 FE code was used to perform the implicit finite-element simulations and the Simulia FE-Safe code was used to calculate the fatigue damage for the notched and cracked specimens. To determine the appropriate mesh size and topology, two convergence analyses were performed. In one convergence analysis the linear brick finite elements C3D8 and the mapped-meshing technique were applied, whereas the parabolic tetrahedron finite elements C3D10 and the free-meshing technique were applied in another analysis. The mesh density was increased around the central hole of the specimen with the element-edge sizes decreasing from 1.0 to 0.075 mm. The best trade-off between the complexity of the FE model, the processing time and the post-processing time for obtaining the fatigue-related results was achieved with a free-mesh using the C3D10 parabolic tetrahedrons, where the local size around the central hole was 0.15 mm. The corresponding mesh for the un-cracked specimen is presented in Fig. 6. It is composed of approximately 107,000 C3D10 finite elements and 157,000 nodes.

Fig. 6: FE model of a notched specimen for simulating a fatigue-crack growth

In all the finite-element simulations the elastic-plastic material model was used, with a Young's modulus E =210 GPa and a Poisson's ratio of 0.3. The true-stress–true-strain $\widetilde{\sigma} - \widetilde{\varepsilon}$ piece-wise linear plasticity curve was defined in Abaqus on the basis of the modelled cyclic curve from Fig. 5 using the well-known transformation between the engineering and the true stresses and strains:

$$\widetilde{\sigma} = \sigma \cdot (1 + \varepsilon) \tag{22}$$

$$\widetilde{\varepsilon} = \ln(1 + \varepsilon) \tag{23}$$

The plastic curve in Abaqus was extended to 100% true plastic strain according to the Ramberg-Osgood model from Section 3.1.

The FE model of the specimen was clamped on one side and a pressure was applied to the other side. By varying the pressure's magnitude and sign, different axial forces acting on the specimen were modelled. The FE simulations were composed of two load steps. In the first load step the peak tensile force was applied to the specimen, which was followed by the application of the peak compressive force in the next step. In this manner a fully reversal loading cycle was simulated.

The output of the Abaqus simulation was imported into the Simulia FE-Safe software for calculating the fatigue damage. The Coffin-Manson curve from Section 3.1 was defined in Simulia FE-safe and was combined with a critical-plane approach for the fatigue-damage predictions. To account for the surface roughness of the specimen, a surface-finish notch factor of 1.05 was considered.

The fatigue-crack propagation process was modelled iteratively by deleting the critically damaged finite elements. To delete the finite elements, the average damage within a finite element should be 0.3 for the given number of loading cycles. The finite elements were deleted manually, which was followed by re-meshing of the crack's geometry. It turned out from the preliminary convergence analysis and the considered criterion for the finite-element annihilation that the crack's propagation could also be reasonably well modelled, if a 0.15-mm-thick layer of the finite elements is deleted in each iteration. This means that the crack was perpendicular to the longitudinal axis of the specimen and grew symmetrically from the middle hole towards the edges of the specimen. The propagating crack width was 0.15 mm and its tip radius was 0.075 mm (see Fig. 6 below).

The specimen was considered broken after the cracks on both sides of the hole reached half the distance to the specimen edge. At each iteration, the number of load cycles that produce 0.15 mm of crack propagation was recorded. The calculated number of load cycles for the un-cracked specimen represented the crack-initiation phase. The cumulative number of load cycles, which resulted from simulating the crack growth, represented the crack-propagation phase.

The crack-growth simulations were performed for three loading levels with the amplitude forces of F_a = 5187 N, 3783 N and 2379 N. The corresponding nominal amplitude stresses in the critical cross-section of the notched specimen were σ_a = 332.5 MPa, 242.5 MPa and 152.5 MPa. The magnitude of the maximum force amplitude was selected in such a manner that the stress concentration near the notch was 5% smaller than the yield stress from the cyclic curve. The magnitude of the minimum force amplitude should result in a notched stress that is above the fatigue-endurance limit for the base material. For example, a strain field in the un-cracked specimen with the calculated fatigue damage during one load cycle is presented for the peak tensile force of

3783 N in Fig. 7. In Fig. 8, the strain field in the cracked specimen with the calculated fatigue damage during one load cycle is presented for the same peak tensile force. In this case the crack length was 0.6 mm on both sides of the central hole.

Fig. 7: Strain distribution and fatigue damage of one load cycle for the amplitude force Fa = 3783 N for the un-cracked specimen

Fig. 8: Strain distribution and fatigue damage of one load cycle for the amplitude force Fa = 3783 N for the cracked specimen with a single crack length of 0.6 mm

The total simulated fatigue lives together with the load cycles of the crack-initiation and crack-propagation phases are presented in Table 1 for the three loading levels. By calculating the linear regression of $\log_{10}(N)$ against $\log_{10}(\sigma_a)$ in Table 1, the slope of the regression line is equal to $a_1 = -6.184$, which is actually the slope of the specimen's synthetic P-S-N curve. It can also be concluded from the numerical results in Table 1 that the crack grows in an elastic-plastic domain at the loading levels 1 and 2. This means that the crack-propagation phase is significant relative to the crack-initiation phase at these loading levels. This is not the case at the third loading level, where the crack-propagation phase represents only 1.5% of the total fatigue life.

Table 1: Simulated fatigue lives for the three loading levels

To determine the intercept a_0 of the specimen's synthetic S-N curve, two notched specimens from Fig. 3 were cut with the water-jet machine from the 2.6-mm-thick sheet-metal plate from the CP800W-equivalent steel in two different directions. They were exposed to the fully reversal, force-controlled fatigue-life experiments at a constant amplitude loading level of $F_a = 5200$ N. Therefore, the nominal amplitude stress in the critical cross-section was $\sigma_a = 333.3$ MPa. The specimens survived 34,115 and 28,058 load cycles until fatigue failure. For the average fatigue life of 31086.5 load cycles to failure at the nominal amplitude stress of $\sigma_a = 333.3$ and the slope $a_1 = -6.184$, it follows from equation (3) that the intercept a_0 of the synthetic specimen's S-N curve is equal to 20.093. By also considering the shape parameter β from the material's S-N curve in Section 3.1, the three parameters $a_0 = 20.093$, $a_1 = -6.184$ and $\beta = 2.440$ could be applied for a preliminary check of the proposed SSALT designs for the notched specimen under consideration.

3.3 Experimental validation of the proposed SSALT designs

The proposed procedure for the SSALT design was tested on two cases of step-stress experiments. In each SSALT design, four equidistant loading levels were defined. To remain within the high-cycle fatigue domain of the notched specimen, the amplitude forces were selected according to the nominal amplitude stresses of $\sigma_a = 174$ MPa, 216 MPa, 258 MPa and 300 MPa. Therefore, the stress increment between the loading levels was 42 MPa. Each loading level also represented a starting

point for a fraction of the specimens. Since the parameters a_0, a_1 and β of the specimen's synthetic P-S-N curve were determined with fully reversal fatigue experiments (see Section 3.2), the proposed SSALTs were also fully reversal and load controlled. To determine the load-cycle block size at each loading level, a trade-off should be made between the high acceleration factor and the possibility of having too many censored data. Namely, if the load-cycle block sizes are small, a lot of specimens can reach the limit condition at the highest loading level $S_{i\,\max}$. This results in a lot of type-I censored data, which reduces the confidence of the experimentally estimated parameters a_0, a_1 and β. For this reason, it was decided that the load-cycle block size will be 100,000 load cycles for the highly accelerated SSALT design (SSALT_1) and 400,000 load cycles for the moderately accelerated SSALT design (SSALT_2). In each SSALT design, the starting loading levels of the notched specimens are distributed between the smallest and the highest loading levels. If a specimen reaches the load-cycle block size at the highest loading level the fatigue experiment is terminated. The two SSALT designs are presented in Fig. 9 and Fig. 10. To test the appropriateness of the two proposed SSALT designs, simulations were made for the synthetic parameters a_0, a_1 and β. For each SSALT design, 16 experiments (4 at every starting level) were simulated according to the procedure from Section 2.1. The results for the simulated data are presented in Table 2. For the simulated data, the acceleration factor of the SSALT_1 design was 3.61 and for the SSALT_2 design it was 1.81.

Fig. 9: SSALT_1 design with the 26 experimentally determined data for the notched specimen

Fig. 10: SSALT_2 design with the 18 experimentally determined data for the notched specimen

Table 2: Simulated results for the two SSALT designs

The notched specimens presented at the bottom of Fig. 3 were cut from the CP800W-equivalent steel sheet-metal plate in three different orientations relative to the axis of rolling. As before, the specimens were not additionally treated to reduce their roughness. All the fatigue-life experiments were carried out on the MTS Landmark 100-kN hydraulic machine. The experiments were fully reversal and load controlled.

The experimental data for the SSALT_1 design consisted of 26 experiments: 10 experiments started at the first loading level (σ_a = 174 MPa), 4 experiments started at the second loading level (σ_a = 216 MPa), 6 experiments started at the third loading level (σ_a = 258 MPa) and 6 experiments started at the fourth loading level (σ_a = 300 MPa). The experimental results are presented with markers in Fig. 9. The SSALT_1 design was tested very thoroughly to find out whether this test design would really result in fatigue failures only at the two highest loading levels, but still with few (or possibly no) censored data. The SSALT_2 design consisted of 18 experiments, with 4 experiments starting at the

first, second and third loading levels and 6 experiments starting at the fourth loading level. The experimental results from SSALT_2 are presented with markers in Fig. 10.

To draw conclusions about the appropriateness of the two proposed SSALT designs, an additional 22 fatigue-life experiments with a constant amplitude loading were conducted for these notched specimens. The nominal amplitude stresses σ_a were in the range 179–333.3 MPa. The results of the constant-amplitude tests for the notched specimens together with the S-N curves for 2.5%, 50% and 97.5% failure probabilities are presented in Fig. 11. The parameters of this P-S-N curve were determined according to Klemenc [19, 38].

Fig. 11: P-S-N curves for the notched specimens with the 22 fatigue-life data

4 Results and discussion

From the results in Table 2, Fig. 9 and Fig. 10 it can be concluded that it was possible to predict the outcomes of the SSALT experiments on the basis of the synthetic P-S-N curve. For both the SSALT_1 and SSALT_2 designs the experimental fatigue failures occurred at the same loading levels as predicted by the simulated data. Also, the distributions of the fatigue-life failures at the individual loading levels S_i are similar for the experimental and the simulated data. Last, but not least, the simulations predicted that no SSALT experiment should result in censored data, which was confirmed by the experiments, despite the fact that more SSALT experimental than simulated data points were obtained. This means that the FE-based synthetic P-S-N curve of the structural part with a single failure mode represents a good starting point for the SSALT design.

The parameters a_0, a_1 and β of the experimental P-S-N curves for the two SSALT designs were determined based on the measured data in Fig. 9 and Fig. 10 with the procedure described in Section 2.2. They are presented in Table 3 together with the experimentally determined parameters a_0, a_1 and β from the constant-amplitude loading for the notched specimen. A comparison of the corresponding median S-N curves (i.e., the S-N curves with a 50% failure probability) is presented in Fig. 12 together with the simulated fatigue-life data. The general observation linked to the data in Table 3 is that the experimentally determined parameters a_0, a_1 and β agree well with the parameters of the specimen's synthetic P-S-N curve, which further confirms the validity of the proposed approach.

Fig. 12: Agreement between the experimental S-N curves for the notched specimen that were determined with different experimental designs

Table 3: Parameters of the experimentally determined P-S-N curves for the notched specimen

From these data it can be concluded that the agreement between the S-N curves that were determined with the SSALT_2 design and the constant-amplitude tests is good. Through the whole high-cycle fatigue domain the median S-N curve for the SSALT_2 data lies within the 95% scatter band of the S-N for the constant-amplitude data. This is a consequence of the fact that the parameters a_0, a_1 for the two P-S-N curves are similar. However, the smaller value of the Weibull's shape coefficient β indicates that the scatter of the experimental data was greater for the SSALT_2 experiments than for the constant-amplitude experiments, which is often the case when a limited number of fatigue-life experiments are performed.

The median S-N curve that was determined with the SSALT_1 experiments has a smaller slope than the median S-N curve from the constant-amplitude experiments. The consequence of this is that the median S-N curve from the SSALT_1 data falls outside the 95% scatter band of the S-N for the constant-amplitude data near the fatigue-endurance domain. Nevertheless, it lies within this scatter band in most of the high-cycle fatigue domain and it intersects the other two experimental S-N curves in the middle of the high-cycle fatigue domain. This means that the estimated fatigue lives and/or reliabilities of the specimen would be acceptable even in the case of the highly accelerated SSALT_1 design. The reason for such a result is that all the fatigue failures were only at the third and fourth loading levels for the SSALT_1 design. Consequently, the SSALT_1 results pushed the S-N parameter a_1 towards more negative values during the optimisation process, despite the fact that the scatter of the fatigue lives was comparable to the constant-amplitude experiments (i.e., the two Weibull's shape parameters β were very similar). This fact suggests that a lower limit for the load-cycle block size N_{tot} need to be carefully chosen. From the presented results it follows that the SSALT scheme should be composed in such a manner that the fatigue failures should occur at more than 50% of the selected loading levels S_i for a reliable estimation of the component's S-N curve. A fulfilment of this criterion can be checked by simulating the SSALT experiments on the basis of the component's synthetic P-S-N curve as presented in section 2.1.

For each of the three sets of experimental data the confidence intervals were determined for the median S-N curves according to the procedure in Section 2.3. The confidence intervals were two-sided for a risk level of 5%. To enable a comparison of the three confidence intervals they were determined for $n = 20$ data points in each case - see Fig. 13.

Fig. 13: Comparison of the 5% confidence limits for the notched specimen's median S-N curves

It can be concluded from Fig. 13 that the narrowest confidence interval is for the constant-amplitude data. This is a consequence of the fact that: i.) the fatigue failures were uniformly distributed along the range of the high-cycle fatigue domain and ii.) the scatter of the results was relatively small, which resulted in the Weibull's shape parameter of β =2.893. Despite the greater scatter of the

fatigue-life data in the SSALT_2 design, when compared to the SSALT_1 design, the confidence interval for the SSALT_2 design is smaller than that for the SSALT_1 design in the lower part of the high-cycle fatigue domain. This is because the fatigue failures occurred at three loading levels for the SSALT_2 design and at only two loading levels for the SSALT_1 design. Despite the confidence interval for the SSALT_1 design being very narrow in the middle part of the high-cycle fatigue domain, it is still better to design the SSALT procedure in such a way that the fatigue failures occur at more loading levels. Then the parameters a_0, a_1 and β of the specimen or component's P-S-N curves are more accurately estimated.

5 Conclusion

The objective of this study was to show how a SSALT can be designed for testing the fatigue life and reliability of structural components with a single failure mode if no prior knowledge on its durability exists. For this purpose, an effective procedure was presented that combines FE simulations with very few fatigue-life experiments to determine the parameters of the component's synthetic P-S-N curve. The P-S-N curve is based on the Weibull's probability distribution with a constant shape factor β and a scale factor η that is linked to the loading level using the inverse power law. With a synthetic P-S-N curve, different SSALT designs can be simulated before the most appropriate one is selected. In this way the possibility of misjudging the loading levels and the load-cycle block sizes can be significantly reduced. The main findings of the study can be summarised as follows:

1. With FE simulations a good estimate of the slope parameter a_1 for the component's P-S-N curve is obtained if the fatigue life considers the crack-initiation and propagation phases.
2. Only a very small number of the fatigue-life experiments are needed to provide a good estimate of the intercept parameter a_0 for the component's S-N curve. Moreover, the material's shape factor β is also a reasonable estimate for the component's shape factor β.
3. When designing the SSALT a trade-off should be made between the high acceleration factor of the test and the accuracy of the estimated component's P-S-N curve. Lower acceleration factors generally yield more accurate P-S-N curves.
4. Last, but not least, the article presents the parameters of the experimentally determined cyclic, Coffin-Manson and P-S-N curves for an advanced, high-strength steel of CP800W-equivalent grade, which are very difficult to find in the literature.

From the presented results it can be concluded that the proposed procedure for designing the SSALT schemes was successfully validated for the case of a single-failure-mode part.

6 References

1. Haibach E. Betriebsfestigkeit: verfahren und Daten zur Bauteilberechnung. 2. Auflage. Heidelberg: Springer Verlag; 2002.
2. Tomazincic D, Necemer B, Vesenjak M, Klemenc J. Low-cycle fatigue life of thin-plate auxetic cellular structures made from aluminium alloy 7075-T651. Fatigue Fract Eng M 2019; 42(5):1022-1036, doi: 10.1111/ffe.12966.
3. Yurkowsky W, Schafer RE, Finkelstein JM. Accelerated testing technology, Volume II: Handbook of accelerated life testing methods. Hughes Aircraft Company; 1967.
4. Escobar LA, Meeker WQ. A Review of Accelerated Test Models. Stat Sci 2006;21: 552–577. https://doi.org/10.1214/088342306000000321.
5. Haiming M. New Developments in Planning Accelerated Life Tests. Ph.D. thesis, Iowa State University: Graduate Theses and Dissertations 11938, 2009. https://lib.dr.iastate.edu/etd/11938 [accessed 16th June 2020)].
6. Chen WH, Gao L, Pan J, Qian P, He QC. Design of Accelerated Life Test Plans - Overview and Prospect. Chin J Mech Eng 2018;31:13, doi: 10.1186/s10033-018-0206-9.
7. W. Nelson. Accelerated testing: statistical models, test plans and data analysis. Hoboken, New Jersey: John Wiley & Sons; 2004.
8. Cheon S, Jeong H, Hwang SY, Hong S, Domblesky J, Kim N. Accelerated Life Testing to Predict Service Life and Reliability for an Appliance Door Hinge. Procedia Manufacturing - 43rd Proceedings of the North American Manufacturing Research Institution of SME 2015;1:169–180.
9. Bunea C, Mazzuchi TA. Competing failure modes in accelerated life testing. J Stat Plan Infer 2006;136:1608–1620, doi: 10.1016/j.jspi.2004.10.030.
10. Luo W, Zhang CH, Chen X, Tan YY. Accelerated reliability demonstration under competing failure modes. Reliab Eng Syst Safe 2015;136:75–8, doi: 10.1016/j.ress.2014.11.014.
11. Nasir EA, Pan R. Simulation-based Bayesian optimal ALT designs for model discrimination. Reliab Eng Syst Safe 2015;134:1–9, doi: 10.1016/j.ress.2014.10.002.
12. Sha N. Statistical Inference for Progressive Stress Accelerated Life Testing with Birnbaum-Saunders Distribution. Stats 2018;1:189–203, doi: 10.3390/stats1010014.
13. Mattetti M, Molari G, Sedoni E. Methodology for the realisation of accelerated structural tests on tractors. Biosyst Eng 2012;113:266-271, doi: 10.1016/j.biosystemseng.2012.08.008.

14. Dimitris S. Paraforos, Hans W. Griepentrog, Stavros G. Vougioukas. Methodology for designing accelerated structural durability tests on agricultural machinery. Biosyst Eng 2016;149:24-37, doi: 10.1016/j.biosystemseng.2016.06.004.
15. Putra TE, Abdullah S, Schramm D, Nuawi MZ, Bruckmann T. Reducing cyclic testing time for components of automotive suspension system utilising the wavelet transform and the Fuzzy C-Means. Mech Syst Signal Pr 2017;90:1–14. , doi: 10.1016/j.ymssp.2016.12.001.
16. Shafiullah AKM, Wu CQ. Generation and validation of loading profiles for highly accelerated durability tests of ground vehicle components. Eng Fail Anal 2013;33:1–16, doi: 10.1016/j.engfailanal.2013.04.008.
17. Lu Y, Zheng H, Zeng J, Chen T, Wu P. Fatigue life reliability evaluation in a high-speed train bogie frame using accelerated life and numerical test. Reliab Eng Syst Safe 2019;188:221-232, doi: 10.1016/j.ress.2019.03.033.
18. ASTM E 739-91: Standard practice for statistical analysis of linear or linearized stress-life (S-N) and strain-life (ε-N) Fatigue Data. ASTM International; 2006.
19. Klemenc J. Influence of fatigue–life data modelling on the estimated reliability of a structure subjected to a constant-amplitude loading. Reliab Eng Syst Safe, 2015;142:238–247, doi: 10.1016/j.ress.2015.05.026.
20. Weibull W. A statistical distribution function of wide applicability. J Appl Mech-Trans ASME 1951;18(3):293–297.
21. Li C. Optimal step-stress plans for accelerated life testing considering reliability/life prediction. Ph.D. thesis. Northeaster University, Boston, Massachusetts; 2009. https://repository.library.northeastern.edu/files/neu:1484/fulltext.pdf [accessed 16th June 2020].
22. Liu X. Bayesian designing and analysis of simple step-stress accelerated life test with Weibull lifetime distribution. M.Sc. thesis. Russ College of Engineering and Technology; 2010. https://etd.ohiolink.edu/!etd.send_file?accession=ohiou1283365980&disposition=inline [accessed 16th June 2020].
23. Mohie El-Din MM, Abu-Youssef SE, Ali NSA, Abd El-Raheem AM. Parametric inference on step-stress accelerated life testing for the extension of exponential distribution under progressive type-II censoring. Commun Stat Appl M 2016;23(4):269–285, doi: 10.5351/CSAM.2016.23.4.269.
24. Hakamiopur N, Rezaei S. Optimising the simple step stress accelerated life test with type I censored Frechet data. REVSTAT – Stat J 2017;15(1):1-23.

25. Abd-Elfattah, AM, Hassan AS, Nassr SG. Estimation in step-stress partially accelerated life tests for the burr type XII distribution using type I censoring. Stat Methodol 2008;5(6):502-514, doi: 10.1016/j.stamet.2007.12.001.
26. Yuan T, Liu X, Kuo W. Planning simple step-stress accelerated life tests using Bayesian methods. IEEE T Reliab 2012;61(1):254-263, doi: 10.1109/TR.2011.2170104.
27. Arefi A, Razmkhah M. Optimal simple step-stress plan for type-I censored data from geometric distribution. J Iran Stat Soc 2013;12:(2):193-210.
28. Tang Y, Guan Q, Xu P, Xu H. Optimum design for type-I step-stress accelerated life tests of two-parameter Weibull distributions. Commun Stat-Theor M, 2012;41:3863–3877, doi: 10.1080/03610926.2012.707456.
29. Xu X, Hunt S. Robust designs of step-stress accelerated life testing experiments for reliability prediction. Matematika 2013;29(1c): 203-212.
30. Wang H, Wang G, Duan F. Planning of step-stress accelerated degradation test based on the inverse Gaussian process. Reliab Eng Syst Safe 2016;154:97–105, doi: 10.1016/j.ress.2016.05.018.
31. Nelson W. Accelerated life testing – step-stress models and data analyses. IEEE T Reliab 1980;R-29(2):103-108.
32. Lee Y, Lu M. Damage-based models for step-stress accelerated life testing. J Test Eval 2006;34:(6):494-503, doi: 10.1520/JTE100172.
33. Stephens RI, Fatemi A, Stephens RR, Fuchs HO Metal fatigue in engineering. 2nd edition. New York: John Wiley & Sons; 2001.
34. Klemenc J, Fajdiga M. Joint estimation of E-N curves and their scatter using evolutionary algorithms. Int J Fatigue 2013;56:42-53, doi: 10.1016/j.ijfatigue.2013.08.005.
35. Franko M, Sedlacek M, Podgornik B, Nagode M. Validation of linear damage rules using random loading. Int J Damage Mech, 2017;26(3):463–479, doi: 10.1177/1056789515605881.
36. Nelson W, Meeker WQ. Theory for optimum accelerated censored life tests for Weibull and extreme value distributions. Technometrics 1978;20(2):171-177.
37. Pascual FG, Meeker WQ, Estimating fatigue curves with the random fatigue-limit model. Technometrics 1999;41(4):277-290, doi: 10.2307/1271342.
38. Klemenc J. Estimating S-N curves with scatter. Executable file for Windows 8/10, http://lab.fs.uni-lj.si/lavek/index.php/sl/predstavitev-laboratorija/osebje/doc-dr-jernej-klemenc-univ-dipl-in-str [accessed 16th June 2020].

39. Harter HL, Moore AH. Asymptotic variances and covariances of maximum-likelihood estimators, from censored samples, of the parameters of Weibull and gamma populations. Ann Math Stat 1967;38(2):557-570.
40. Thoman DR, Bain LJ, Antle CE. Maximum likelihood estimation, exact confidence tntervals for reliability, and tolerance limits in the Weibull distribution. Technometrics 1970;12(2):363-371.
41. McCool JI. Confidence limits for Weibull regression with censored data. IEEE T Reliab 1980;R-29:(2):145-150.
42. Phan LD, McCool JI. Exact confidence intervals for Weibull parameters and percentiles. P IMechE O: J Risk Reliab 2009;223:387-394, doi: 10.1243/1748006XJRR247.
43. Meeker WQ, LA Escobar. Statistical methods for reliability data. New York: John Wiley & Sons; 1998.
44. ASTM E 606-92: Standard practice for strain-controlled fatigue testing. ASTM International; 1996.
45. Seruga D, Nagode M, Klemenc J. Eliminating friction between flat specimens and an antibuckling support during cyclic tests using a simple sensor. Meas Sci Technol 2019;30(9):1–23, doi: 10.1088/1361-6501/ab1e35.

Acknowledgment

This research was funded by the Slovenian Research Agency (ARRS), grant research programme P2-0182 (R&D evaluations – Razvojna vrednotenja).

Conflict of interest

The authors declare that they have no known competing financial interests or personal relationships that could have appeared to influence the work reported in this paper.

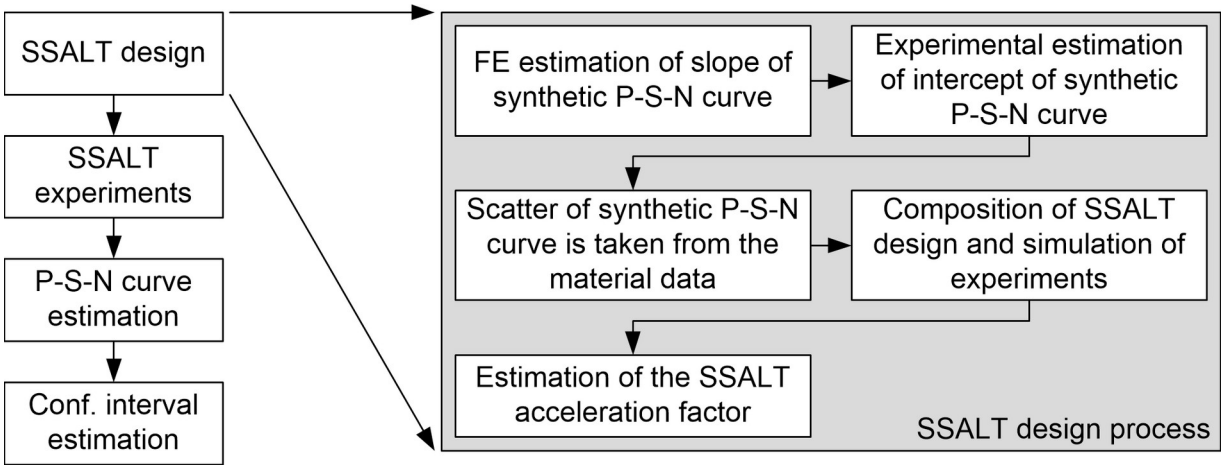

Fig. 1: Estimating the component's P-S-N curve via SSALT experiments

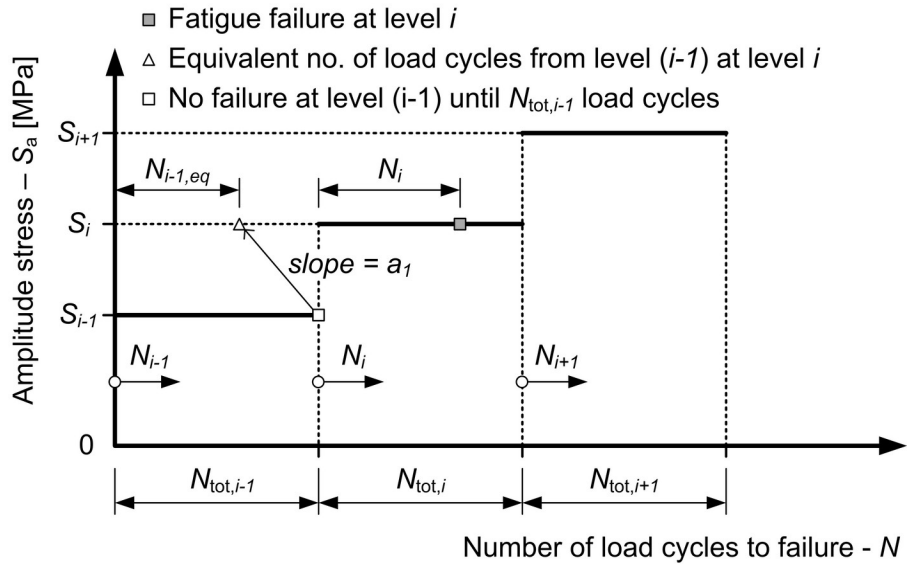

Fig. 2: SSALT test plan and the calculation of the equivalent number of load cycles

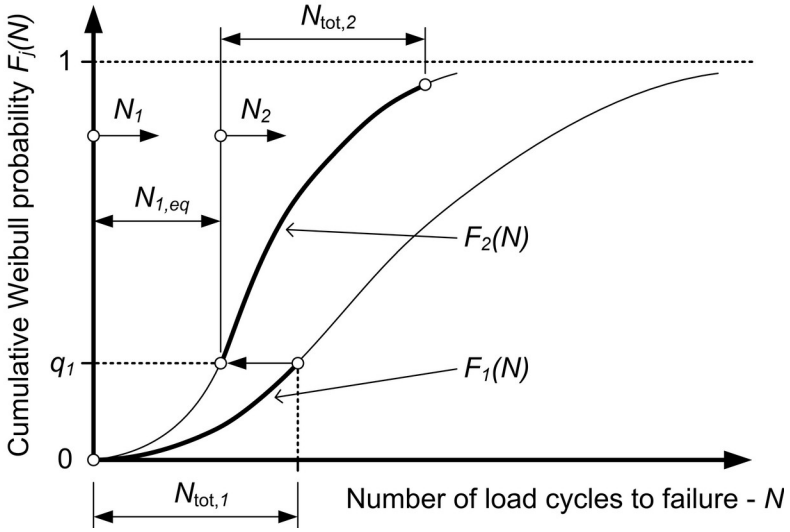

Fig. 3: Determination of the cumulative density function during the SSALT data processing

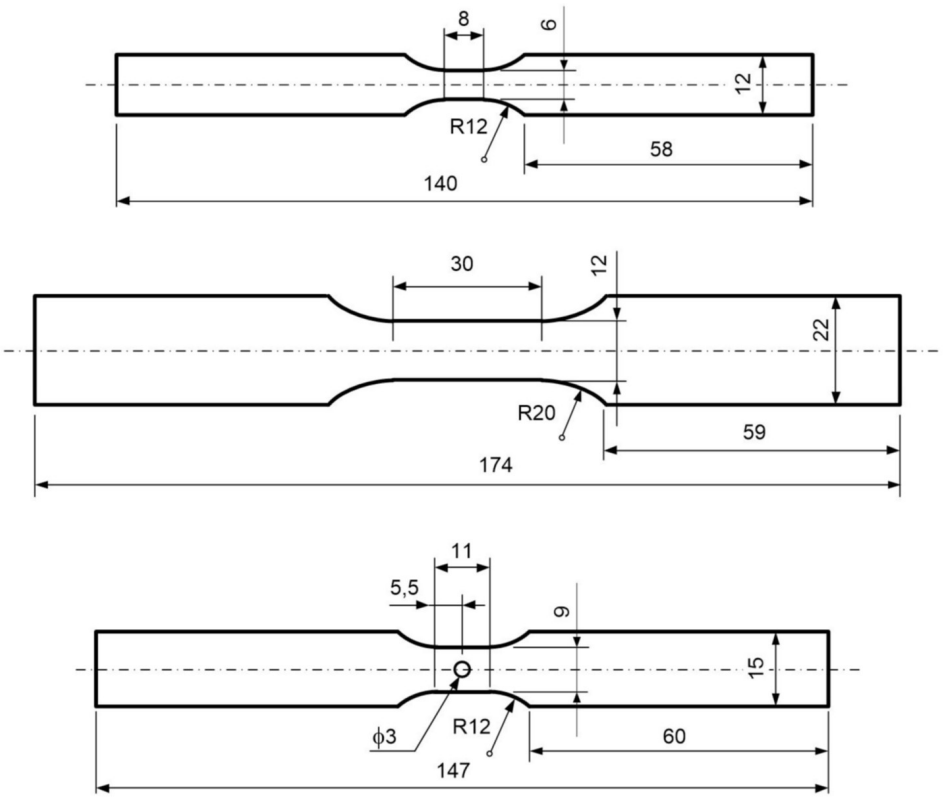

Fig. 4: Smooth specimen geometries for high-cycle fatigue testing (top), static and low-cycle fatigue testing (middle) and notched specimen geometry for high-cycle fatigue testing (bottom)

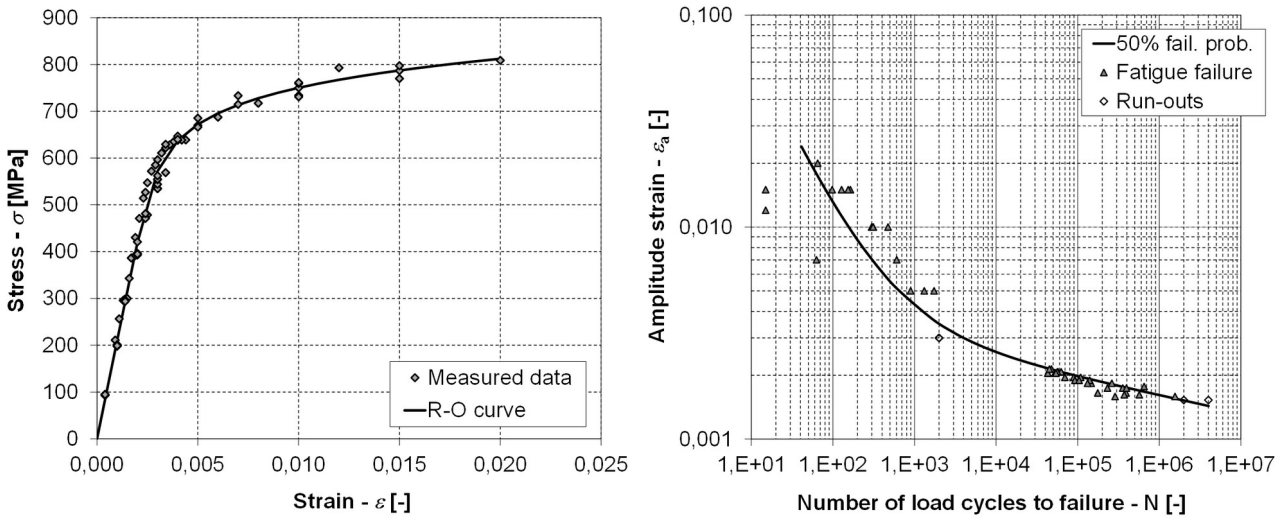

Fig. 5: Cyclic curve (left) and Coffin-Manson curve (right) for the CP800W-equivalent steel

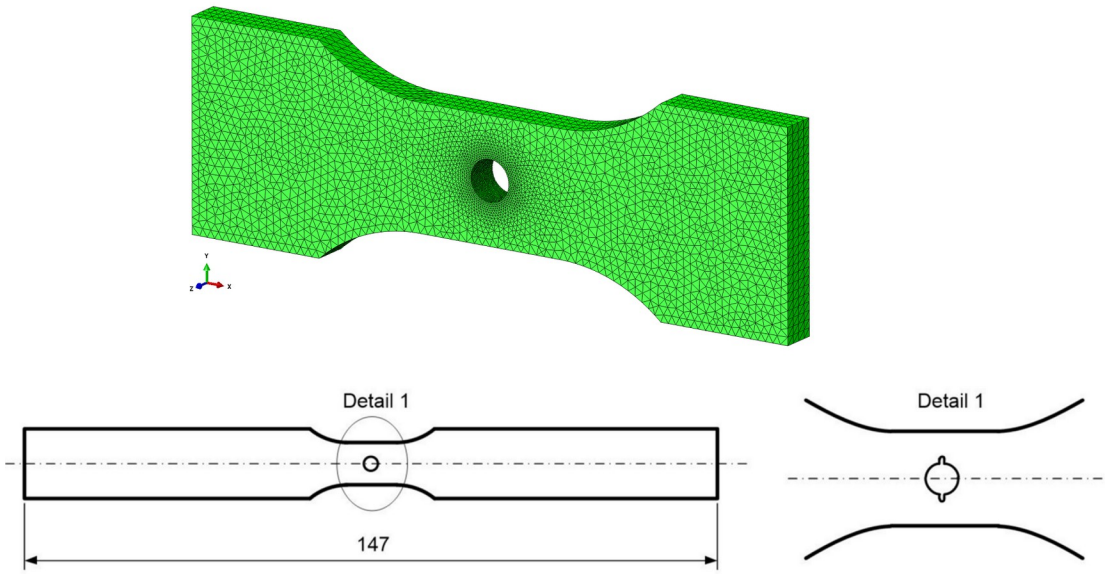

Fig. 6: FE model of a notched specimen for simulating a fatigue-crack growth

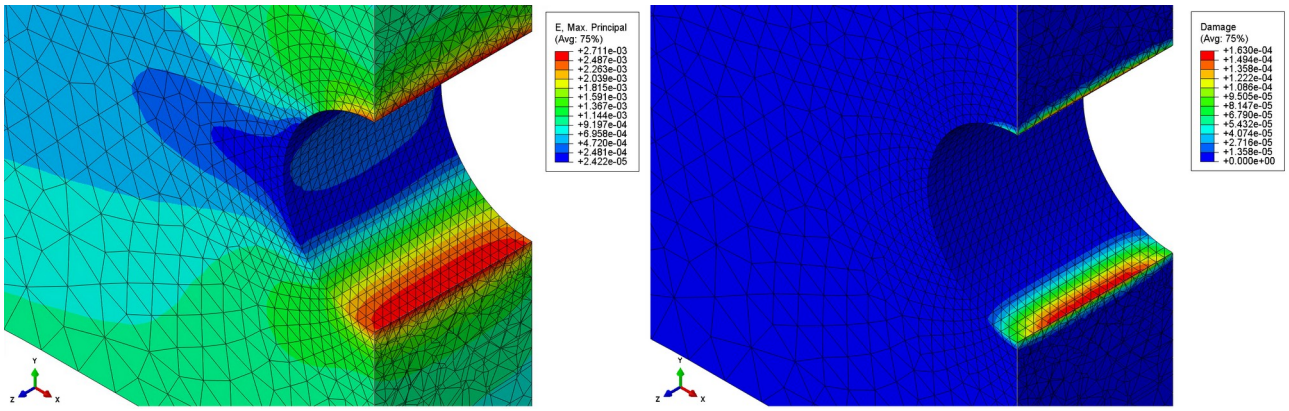

Fig. 7: Strain distribution and fatigue damage of one load cycle for the amplitude force F_a = 3783 N for the un-cracked specimen

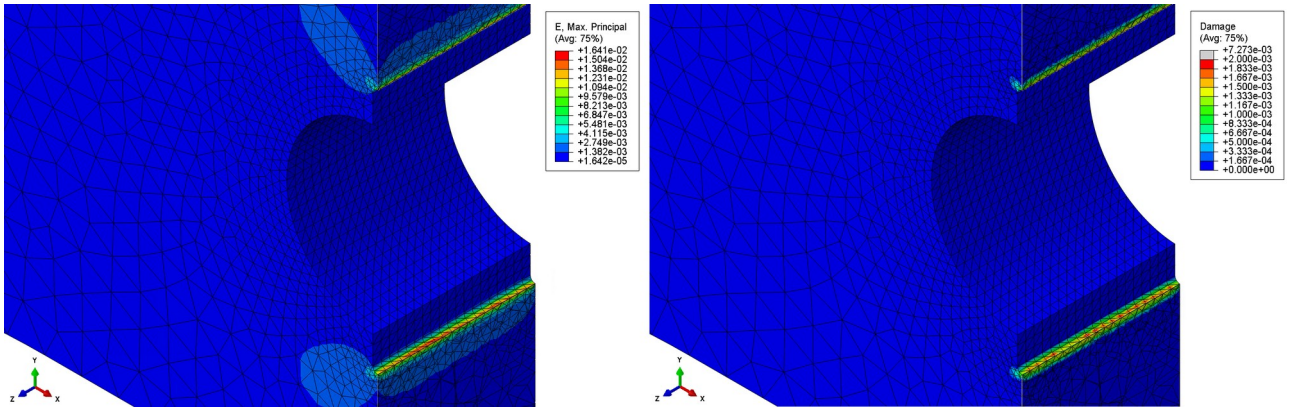

Fig. 8: Strain distribution and fatigue damage of one load cycle for the amplitude force F_a = 3783 N for the cracked specimen with a single crack length of 0.6 mm

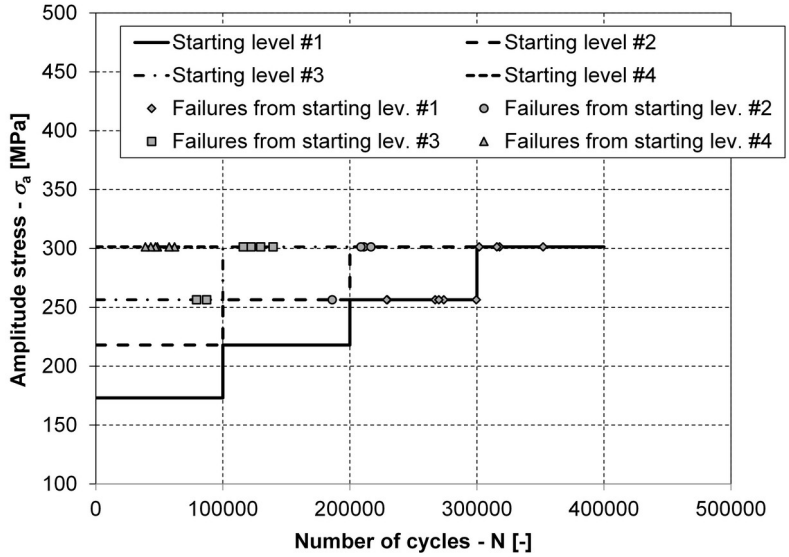

Fig. 9: SSALT_1 design with the 26 experimentally determined data for the notched specimen

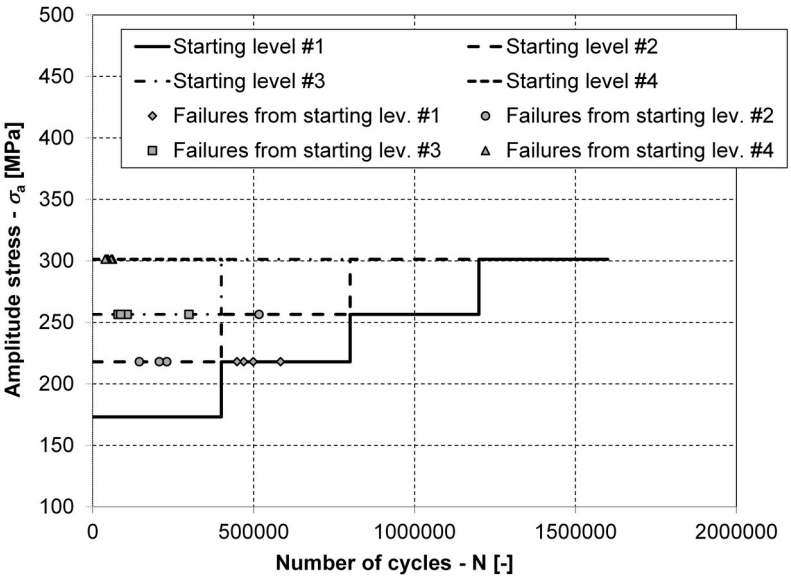

Fig. 10: SSALT_2 design with the 18 experimentally determined points for the notched specimen

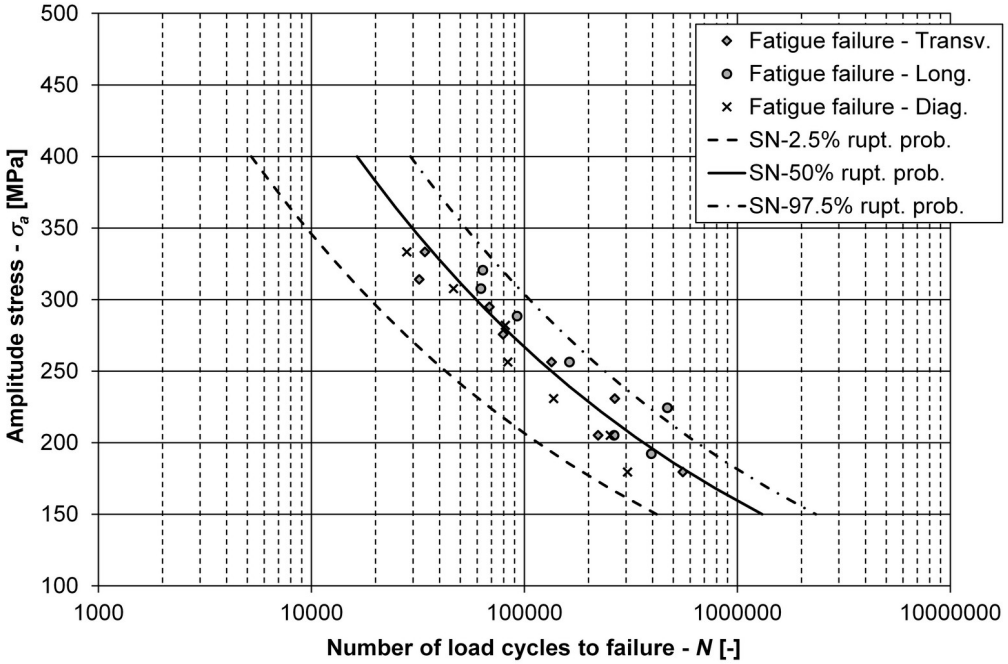

Fig. 11: P-S-N curves for the notched specimens with the 22 fatigue-life data

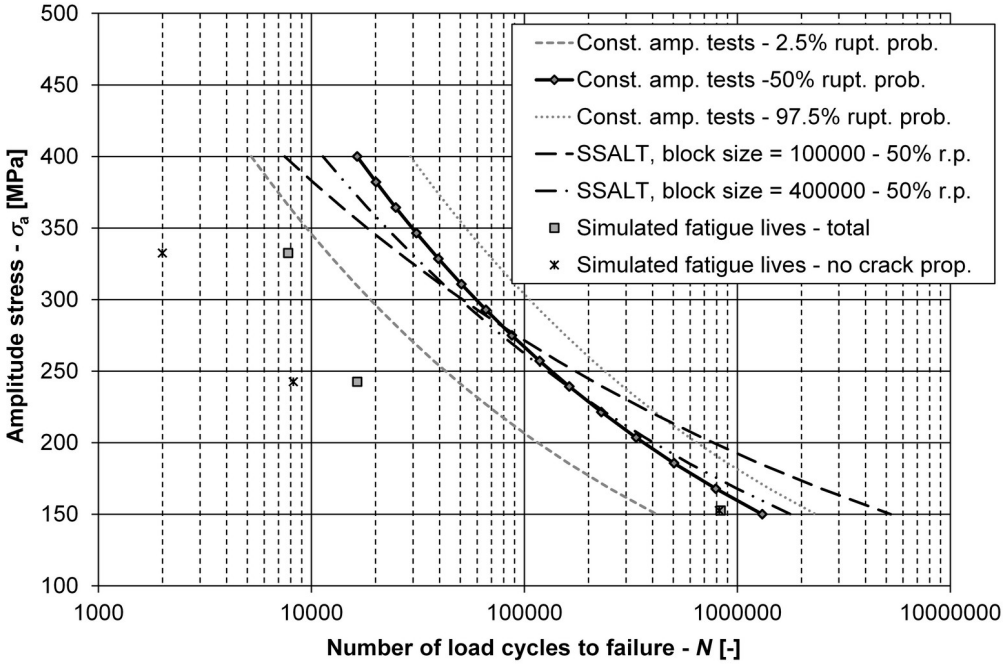

Fig. 12: Agreement between the experimentally determined S-N curves for the notched specimens that were determined with different experimental designs

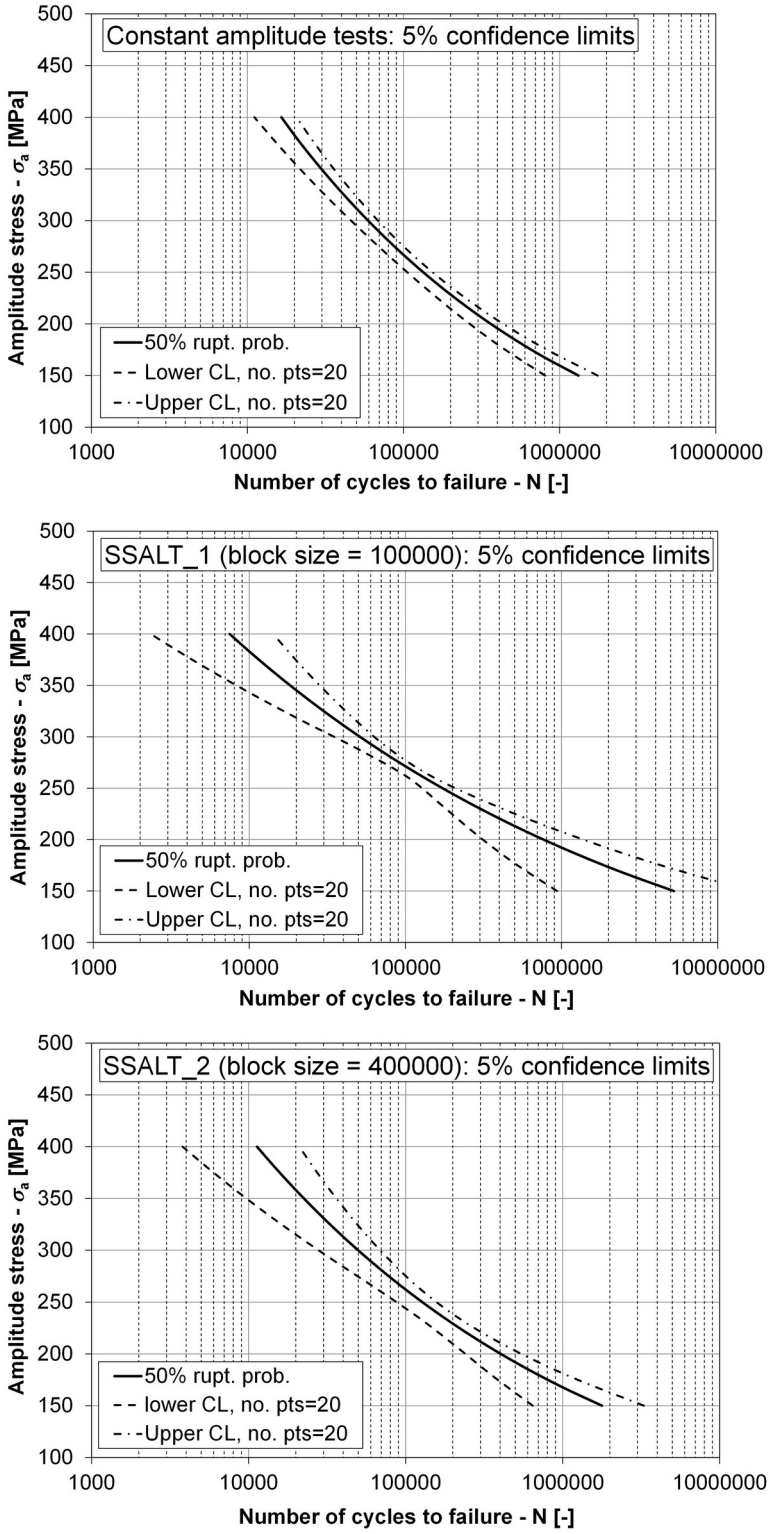

Fig. 13: Comparison of the 5% confidence limits for the notched specimen's median S-N curves

Table 1: Simulated fatigue lives for the three loading levels

Loading level	Force amplitude	Nominal stress amplitude	Calculated number of loading cycles		
	F_a [N]	σ_a [MPa]	N_{tot} [-]	N_{init} [-]	N_{prop} [-]
1	5187	332.5	7783	1998	5785
2	3783	242.5	16411	8230	8181
3	2379	152.5	835610	823045	12565

Table 2: Simulated results for the two SSALT designs

SSALT design	Starting loading level	Load-cycle block size	Loading levels at fatigue failure	Acceleration factor
	$\sigma_{a,/min}$ [MPa]	$N_{tot.i}$ [-]	l [-]	AF [-]
SSALT_1	174 (4)*	100000	4, 3, 4, 3	3.61
	216 (4)*	100000	4, 3, 3, 3	
	258 (4)*	100000	4, 4, 4, 4	
	300 (4)*	100000	4, 4, 4, 4	
SSALT_2	174 (4)*	400000	3, 2, 3, 2	1.81
	216 (4)*	400000	3, 2, 2, 2	
	258 (4)*	400000	3, 3, 3, 3	
	300 (4)*	400000	4, 4, 4, 4	

* Number of specimens, for which the SSALT experiment started at this loading level.

Table 3: Parameters of the experimentally determined P-S-N curves for the notched specimen

Experimental arrangement	Intercept	Slope	Weibull's shape factor
	a_0 [-]	a_1 [-]	β [-]
Constant-amplitude test	15.892	-4.467	2.893
SSALT_1	21.309	-6.681	3.156
SSALT_2	17.558	-5.157	1.875